

CORONARY ANGIOGRAPHY

## Initial Experiences with In Vivo Right Coronary Artery Human MR Vessel Wall Imaging at 3 Tesla

René M. Botnar, Ph.D.,<sup>1,3,\*</sup> Matthias Stuber, Ph.D.,<sup>1,3</sup> Rolf Lamerichs, Ph.D.,<sup>3</sup>  
Jouke Smink, M.Sc.,<sup>3</sup> Stefan E. Fischer, Ph.D.,<sup>3</sup> Paul Harvey, Ph.D.,<sup>3</sup> and  
Warren J. Manning, M.D.<sup>1,2</sup>

<sup>1</sup>Department of Medicine, Cardiovascular Division, and <sup>2</sup>Department of Radiology, Beth Israel Deaconess Medical Center and Harvard Medical School, Boston, USA

<sup>3</sup>Philips Medical Systems, Best, The Netherlands

### ABSTRACT

Due to their relatively small size and central location within the thorax, improvement in signal-to-noise (SNR) is of paramount importance for in vivo coronary vessel wall imaging. Thus, with higher field strengths, coronary vessel wall imaging is likely to benefit from the expected “near linear” proportional gain in SNR. In this study, we demonstrate the feasibility of in vivo human high field (3 T) coronary vessel wall imaging using a free-breathing black blood fast gradient echo technique with respiratory navigator gating and real-time motion correction. With the broader availability of more SNR efficient fast spin echo and spiral techniques, further improvements can be expected.

*Key Words:* Vessel wall; High field; Magnetic resonance; Coronary artery; Atherosclerosis.

### INTRODUCTION

Apart from cardiac and respiratory motion, the major obstacle to coronary magnetic resonance (MR) vessel wall imaging is the relatively small thickness of the coronary artery wall (0.5–2 mm) and thus the need

for high spatial resolution. In the past, the use of signal-to-noise (SNR) optimized three-dimensional MR imaging sequences (Botnar et al., 2001) or dedicated phase array coils (Fayad et al., 2000b) has been explored to meet these demands. In theory, SNR is directly proportional to field strength. Thus, with the broader

\*Correspondence: René M. Botnar, Ph.D., Department of Medicine, Cardiovascular Division, Beth Israel Deaconess Medical Center and Harvard Medical School, 330 Brookline Ave, Boston, MA 02215, USA; Fax: 617-975 5480; E-mail: rbotnar@caregroup.harvard.edu.



availability of higher field whole body MR systems, in vivo coronary vessel wall imaging is likely to benefit from the expected proportional increase in SNR (Dougherty et al., 2001; Singerman et al., 1997). Improved SNR could either be used to enhance spatial resolution or to reduce total imaging time.

New challenges associated with higher field systems are increased magnetic field susceptibilities and reduced  $T2^*$  relaxation times (Noeske et al., 2000), which might impair the implementation of two-dimensional selective pulses (commonly used for MR navigators), or make use of SNR-efficient, three-dimensional, spiral sequences more difficult (Botnar et al., 2001). Furthermore, little is known how the decreased radiofrequency (RF) penetration (Wen et al., 1997), increased RF energy deposition (Singerman et al., 1997), or RF-field distortions (Wen et al., 1997) will affect cardiac imaging (Dougherty et al., 2001) or how the magneto hydrodynamic effect will impact electrocardiogram (ECG) triggering. In addition, standing waves due to body dielectric resonances are expected to pose new challenges on the design of receiver coils arrays (Leussler and Röschmann, 1999; Wen et al., 1997). Increased  $T1$  relaxation times of blood (Noeske et al., 2000), myocardium (Noeske et al., 2000), and epicardial fat have to be considered when defining black blood or spectral fat saturation prepulses.

In this study we sought to evaluate the feasibility of free-breathing, navigator-gated and corrected in vivo coronary vessel wall imaging in humans on a commercial, 3 T whole body scanner.

## METHODS

### Subjects

Free-breathing two-dimensional black blood coronary vessel wall imaging was performed in five healthy adult subjects (age:  $44 \pm 8$  yrs, 5 months) using a short-bore (length = 157 cm, diameter = 60 cm) commercial Philips Intera 3 T MR scanner (Philips Medical Systems, Best, The Netherlands). The system was equipped with MASTER<sup>®</sup> gradients (30 mT/m, 150 mT/m/ms), a prototype body send/receive RF-coil, a prototype six-channel, phased array, receiver coil, and an advanced cardiac software package (R8.1.3). Field strength-related parameters such as the  $T1$  relaxation time of blood ( $T1 = 1550$  ms) (Noeske et al., 2000), myocardium ( $T1 = 1150$  ms) (Noeske et al., 2000), and epicardial fat ( $T1 = 290$  ms) at 3 T as well as the frequency offset ( $\Delta f = 440$  Hz) of the fat suppression pre-pulse were adapted. Furthermore, the time delay ( $T_d = 200$  ms) of the fat suppression prepulse (STIR), which is used during

power optimization, had to be adjusted. Written informed consent was obtained from all participants.

## Imaging Protocol

### Localization of the Coronary Arteries

All scanning was performed during uncoached, free breathing. A vector ECG-triggered (Fischer et al., 1999) multi-stack (9 transverse, 9 sagittal, 9 coronal), fast gradient, echo scout scan ( $TR = 9.2$  ms,  $TE = 2.2$  ms,  $\alpha = 30^\circ$ ,  $FOV = 450$  mm, matrix =  $256 \times 128$ , slice thickness = 10 mm) was acquired for localization of the heart and hemidiaphragms: Subsequently, an ECG-triggered, navigator-gated, transverse three-dimensional fast gradient echo-echo planar (TFE-EPI) scout scan was performed for identification of the proximal and mid right coronary artery (RCA). The major axis of the RCA was subsequently defined using a three-point planscan tool (Stuber et al., 1999). Imaging along the major axis of the RCA was then performed using a previously described, navigator-gated and corrected three-dimensional, black blood, coronary MRA sequence (Stuber et al., 2001).

### MR Navigator

The two-dimensional selective navigator beam (NAV) was positioned at the apex of the left ventricle. Prospective gating and real-time motion correction was performed with a 5 mm gating window and a constant superior-inferior correction factor of 0.6 (Wang et al., 1995). To minimize sensitivity of the two-dimensional selective navigator pulse to increased  $B_0$  inhomogeneities and shortened  $T2^*$  values, the RF and gradient waveforms of the navigator were shortened by reducing the excitation trajectory to eight turns in k-space. Navigator signal reception with an anterior synergy coil element (placed on the sternum) minimized signal contributions from sampling rings at the edge of the field-of-view (FOV), which is prone to increased  $B_0$  inhomogeneities.

### Coronary Wall Imaging Sequence

Prospective vector ECG triggering was used for cardiac synchronization, and imaging was performed during mid-diastolic diastasis (Kim et al., 2001). After identification of the long axis of the RCA, navigator-gated and real-time motion corrected cross-sectional views of the RCA were acquired. The MR pulse sequence (Fig. 1) consisted of a double inversion (Dual-



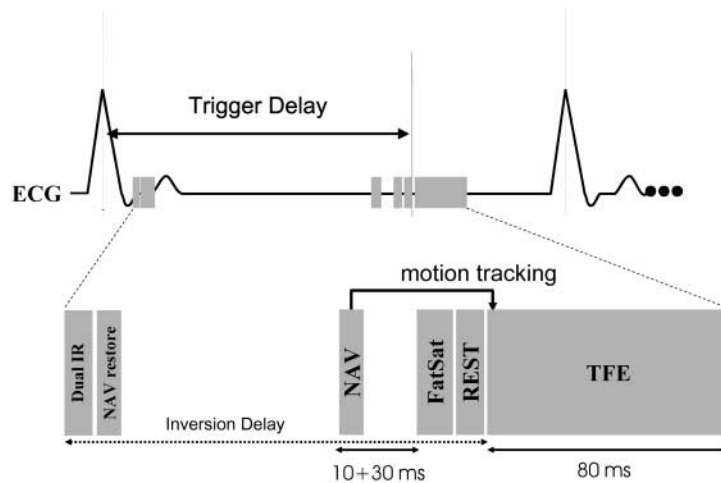


**Figure 1.** Schematic of black blood (TFE) imaging sequence. The mid-diastolic TFE imaging sequence (10 RF excitations, TR = 8 ms) is immediately preceded by a saturation (REST) slab for chest wall signal attenuation, a fat suppression (FatSat) prepulse for epicardial fat suppression, and a 2D selective navigator pulse (NAV) beam for real-time gating and adaptive motion correction. Immediately following the R-wave of the ECG, a double inversion (Dual-IR) prepulse was applied to null blood signal during mid-diastolic imaging followed by a navigator restore (NAV restore) pulse to facilitate navigator gating. *Source:* (Stuber et al., 2001).

IR) black blood prepulse with the inversion delay (TI) (Fleckenstein et al., 1991) adapted for the longer T1 of blood (TI = 698 ms @ 60 bpm). The two-dimensional segmented fast gradient echo TFE imaging sequence was immediately preceded by a two-dimensional selective navigator pulse (NAV), a frequency-selective, fat suppression prepulse (FatSat;  $\alpha = 130^\circ$ ), a saturation slab (REST) for chest wall signal attenuation, and a NAV-restore prepulse for optimization of navigator performance in the presence of a nonselective  $180^\circ$  prepulse. Other imaging parameters included TE = 2.3 ms, TR = 8 ms, bandwidth = 135 Hz/pixel, flip angle =  $30^\circ$ , 10 RF excitations per shot, NSA = 2, FOV = 360 mm, image matrix =  $512 \times 512$  resulting in an in-plane resolution of  $0.7 \times 0.7$  mm, and a slice thickness of 5 mm. Images were reconstructed only from the anterior coil element centered over the sternum, which is in close vicinity of the RCA.

### Data Analysis

SNR and contrast-to-noise (CNR) measurements were performed for each two-dimensional slice. Mean signal values (S) were calculated in regions-of-interest (ROI) drawn in the myocardium, the left ventricular blood pool, the vessel wall, and in epicardial fat. Noise (N) was determined as signal standard deviation (SD) measured in a ROI anterior to the chest wall. The SNR was defined as  $S/N$  and CNR as  $(S_{\text{tissue1}} - S_{\text{tissue2}})/N$ .

To allow for comparison with previous measurements on 1.5T (Botnar et al., 2000), adjustments for spatial resolution, number of signal averages, and the type of imaging sequence were made. Lumen and vessel wall area measurements were performed on cross-sectional images as previously described (Botnar et al., 2000).

## RESULTS

In all subjects, the right coronary artery could be successfully visualized with high contrast between epicardial fat, coronary vessel wall, and coronary blood (Figs. 2, 3). Scanning time was approximately 5 minutes for a two-dimensional slice. The SNR data are listed in Table 1 and compare favorably with values previously obtained on a 1.5T system (Botnar et al., 2000). The CNR between wall and fat was  $9 \pm 2$  and  $11 \pm 4$  between wall and blood. Lumen diameter and vessel wall thickness values (Table 2) are also in good agreement with published 1.5T data for healthy subjects (Botnar et al., 2000; Fayad et al., 2000a). Due to the relatively small number of RF pulses per cardiac cycle, RF heating was not a limiting factor, and RF penetration was sufficient to allow for visualization of the proximal RCA. Although a relatively SNR-inefficient, black blood, TFE sequence was used, good depiction of the coronary vessel wall with an in-plane voxel size of  $700 \times 700 \mu\text{m}$  could be achieved (Figs. 2, 3). The prolonged inversion time of the black blood prepulse resulted in a good suppression



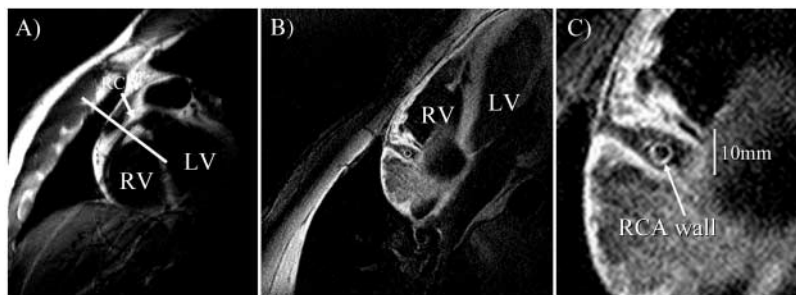


**Figure 2.** The vessel wall scan (B) was planned from a double oblique view (A) of the right coronary artery (RCA). The RCA vessel wall is readily visible on a magnified view (C). Key: RA, right atrium; RV, right ventricle; LV, left ventricle.

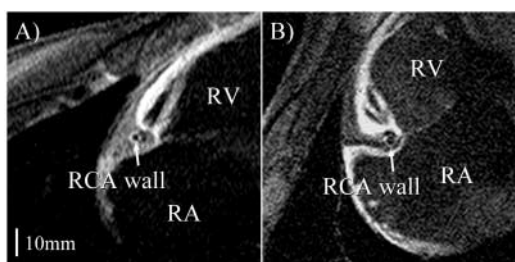


**Figure 3.** Right coronary vessel wall images from two additional subjects. In both cases, the right coronary vessel wall is well delineated with high contrast between the wall and adjacent coronary blood and epicardial fat.

of left and right ventricular intracavitary blood. Suppression of epicardial fat was comparable to a 1.5 T system with frequency offset, flip angle, and prepulse delay time adjusted for the higher field strength (Table 1). We found navigator positioning more critical than on 1.5 T systems, likely due to increased susceptibility artifacts and shortened  $T2^*$  values. Especially at the lung-liver interface, navigator performance with the pencil beam positioned on the dome of the right hemidiaphragm often was poor. By positioning the navigator on the apex of the left ventricle, navigator performance was improved and comparable to earlier 1.5 T experiences (Botnar et al., 2000). In addition, shortening the two-dimensional selective RF pulse

helped minimize the sensitivity to  $\Delta B_0$  and reduced  $T2^*$  relaxation times. The ECG traces showed an increased T-wave (due to the magneto hydrodynamic effect), but the vector ECG algorithm allowed for reliable detection of the R-wave and successful triggering in all cases.

## DISCUSSION

In this study we demonstrate the feasibility of cardiac-triggered and navigator-gated, two-dimensional, coronary vessel wall imaging on a commercial 3 T whole body system. In all subjects, images of the RCA wall could be obtained with good contrast between vessel wall, epicardial fat, and coronary blood. Lumen diameter, lumen area, vessel wall thickness, and vessel wall area could be quantified in all cases and were in good agreement with prior 1.5 T data (Botnar et al., 2000; Fayad et al., 2000a). Although not demonstrated in this study, this technique also should be applicable to the left anterior descending (LAD) and left circumflex (LCX) vessel wall.

### SNR and CNR Considerations

After adjustments for spatial resolution, the number of signal averages, and imaging sequence (Botnar et al.,

**Table 1.** Signal-to-noise (SNR) values of myocardium, vessel wall, ventricular blood, and epicardial fat at 3 T and 1.5 T.

	Myocardium	RCA wall	Blood	Epicardial fat
SNR @ 3 T	$24 \pm 8$	$17 \pm 5$	$5 \pm 1$	$8 \pm 5$
Adjusted SNR @ 3 T†	$38 \pm 8$	$26 \pm 6$	$8 \pm 2$	$12 \pm 5$
SNR @ 1.5 T (Botnar et al., 2000)		$18 \pm 6$	$9 \pm 4$	$9 \pm 6$

† Values adjusted for voxel size, NSA, and type of imaging sequence to allow comparison with prior publication (Botnar et al., 2000).

**Table 2.** Lumen diameter and area—vessel wall thickness and area.

Lumen diameter (mm)	Lumen area (mm <sup>2</sup> )	Wall thickness (mm)	Wall area (mm <sup>2</sup> )
3.2 ± 0.6	8.5 ± 2.9	0.9 ± 0.3	12.2 ± 3.4

2000), SNR gain was approximately 50% when compared to previous studies at 1.5 T (Botnar et al., 2000). The Q-value of the body coil used at 3.0 T (empty condition) was almost twice as high as at 1.5 T. With higher loads, the effective Q-value decreases, and this effect is more pronounced at 3.0 T and therefore might explain the slightly lower than expected gain in SNR. Furthermore, the difference between the measured and expected theoretical value of 100% is likely also due to differences in body size of the subjects, the software releases, and the prolonged T1 and shortened T2\* relaxation times, which might result in additional signal attenuation. Direct comparisons of subjects at 1.5 T and 3 T using common software and receiver coils will facilitate identification of these differences.

### RF Considerations

In normal subjects, neither increased RF deposition nor decreased RF penetration appeared to be a limiting factor. Furthermore, RF-field distortions, which are likely to occur at higher field strengths (Wen et al., 1997), did not visually affect image quality. Due to the relatively low RF duty cycle in coronary vessel wall imaging, imaging with more RF demanding fast spin echo sequences seems to be feasible.

### B<sub>0</sub> Field Inhomogeneities

Shortening the two-dimensional, selective, RF pulse helped minimized the sensitivity to  $\Delta B_0$  and reduced T2\* relaxation times and resulted in a navigator performance similar to that at 1.5 T. Continued improvements in magnet technology leading to improved B<sub>0</sub> field homogeneity are likely to further improve navigator performance.

### Black Blood and Fat Suppression Prepulse—Comparison to 1.5 T

Blood suppression using a dual-IR prepulse and a frequency-selective, fat saturation prepulse was reliable

at 3 T and resulted in good suppression of ventricular blood and epicardial fat. Though only preliminary and with a limited number of subjects, 3 T data regarding SNR and CNR suggest that higher field, coronary vessel wall imaging is promising and thus demands continued study.

### CONCLUSION

We demonstrate the feasibility of higher field (3 T), coronary MR vessel wall imaging using a free-breathing black blood two-dimensional fast gradient echo technique with ECG-triggering and navigator-gating. With growing experience on higher field systems and more experience with fast spin echo and spiral techniques, further improvements towards improved spatial resolution, coronary MR vessel wall imaging can be expected.

### REFERENCES

- Botnar, R. M., Kim, W. Y., Bornert, P., Stuber, M., Spuentrup, E., Manning, W. J. (2001). 3D coronary vessel wall imaging utilizing a local inversion technique with spiral image acquisition. *Magn. Reson. Med.* 46(5):848–854.
- Botnar, R. M., Stuber, M., Kissinger, K. V., Kim, W. Y., Spuentrup, E., Manning, W. J. (2000). Noninvasive coronary vessel wall and plaque imaging with magnetic resonance imaging. *Circulation* 102(21): 2582–2587.
- Dougherty, L., Connick, T. J., Mizsei, G. (2001). Cardiac imaging at 4 Tesla. *Magn. Reson. Med.* 45(1):176–178.
- Fayad, Z. A., Fuster, V., Fallon, J. T., Jayasundera, T., Worthley, S. G., Helft, G., Aguinaldo, J. G., Badimon, J. J., Sharma, S. K. (2000a). Noninvasive in vivo human coronary artery lumen and wall imaging using black-blood magnetic resonance imaging. *Circulation* 102(5):506–510.
- Fayad, Z. A., Hardy, C. J., Giaquinto, R., Kini, A. S., Fuster, V. (2000b). Improved high resolution MRI of human coronary lumen and plaque with a new cardiac coil. *Circulation* 102(Suppl.):II–399.
- Fischer, S. E., Wickline, S. A., Lorenz, C. H. (1999). Novel real-time R-wave detection algorithm based on the vectorcardiogram for accurate gated magnetic resonance acquisitions. *Magn. Reson. Med.* 42(2):361–370.
- Fleckenstein, J. L., Archer, B. T., Barker, B. A., Vaughan, J. T., Parkey, R. W., Peshock, R. M.



- (1991). Fast short-tau inversion-recovery MR imaging. *Radiology* 179(2):499–504.
- Kim, W. Y., Stuber, M., Kissinger, K. V., Andersen, N. T., Manning, W. J., Botnar, R. M. (2001). Impact of bulk cardiac motion on right coronary MR angiography and vessel wall imaging. *J. Magn. Reson. Imaging* 14(4):383–390.
- Leussler, C., Röschmann, P. (1999). 3D simulation of electromagnetic fields inside the human body for applications of MR and EPR: effects of object size and frequency on RF field homogeneity. In: ISMRM'99, 7th Annual Meeting, Philadelphia. International Society for Magnetic Resonance in Medicine: Berkeley, California, USA, p. 2050.
- Noeske, R., Seifert, F., Rhein, K. H., Rinneberg, H. (2000). Human cardiac imaging at 3 T using phased array coils. *Magn. Reson. Med.* 44(6):978–982.
- Singerman, R. W., Denison, T. J., Wen, H., Balaban, R. S. (1997). Simulation of B1 field distribution and intrinsic signal-to-noise in cardiac MRI as a function of static magnetic field. *J. Magn. Reson.* 125(1):72–83.
- Stuber, M., Botnar, R. M., Danias, P. G., Sodickson, D. K., Kissinger, K. V., Van Cauteren, M., De Becker, J., Manning, W. J. (1999). Double-oblique free-breathing high resolution three-dimensional coronary magnetic resonance angiography. *J. Am. Coll. Cardiol.* 34(2):524–531.
- Stuber, M., Botnar, R. M., Spuentrup, E., Kissinger, K. V., Manning, W. J. (2001). Three-dimensional high-resolution fast spin-echo coronary magnetic resonance angiography. *Magn. Reson. Med.* 45(2):206–211.
- Wang, Y., Riederer, S. J., Ehman, R. L. (1995). Respiratory motion of the heart: kinematics and the implications for the spatial resolution in coronary imaging. *Magn. Reson. Med.* 33(5):713–719.
- Wen, H., Denison, T. J., Singerman, R. W., Balaban, R. S. (1997). The intrinsic signal-to-noise ratio in human cardiac imaging at 1.5, 3, and 4 T. *J. Magn. Reson.* 125(1):65–71.

Received August 28, 2002

Accepted June 18, 2003

